

## 3D SIMULATIONS OF INTERNAL GRAVITY WAVES IN STELLAR INTERIORS

L. Alvan<sup>1</sup>, A. S. Brun<sup>1</sup> and S. Mathis<sup>1</sup>

**Abstract.** We investigate the excitation and propagation of internal gravity waves by penetrative convective plumes using the 3D anelastic simulation code ASH. The study of the waves' properties is of high importance for helio- and asteroseismology and to understand how waves transport angular momentum and may establish the observed rotation profile of the solar radiative zone. After illustrating basic properties of g-modes in terms of simple ray-theory, we show that the rich field of gravity waves obtained with our 3D model is in good agreement with theoretical predictions concerning the period spacing of g-modes.

Keywords: Stars, Turbulence, Waves, Methods : Numerical

### 1 Introduction

Internal gravity waves (IGWs) are essential for helio- and asteroseismology to probe stellar interiors (e.g. Garcia et al. 2007). Moreover, they are of great interest in the study of angular momentum transport over large distances (Rogers & Glatzmaier 2005) and constitute an important ingredient in understanding the evolution of stellar rotation (Zahn et al. 1997; Charbonnel & Talon 2005; Mathis 2009). We here present new results obtained with the Anelastic Spherical Harmonic (ASH) code (Brun et al. 2004). Our model nonlinearly couples the convective envelope to the stable radiative interior of the Sun (Brun et al. 2011), assuming a realistic solar stratification from  $r = 0.07R_{\odot}$  up to  $0.97R_{\odot}$  (Brun et al. 2002). The pummeling of convective plumes at the top of the radiative zone generates perturbations which propagate in the stably stratified zone. We show that these perturbations have the characteristics of IGWs predicted by linear theory.

### 2 Raytracing

IGWs propagate in the solar radiative zone under the condition  $\omega < N$  where  $\omega$  is the waves frequency and  $N$  the Brunt-Väisälä frequency, plotted in the left panel of Fig. 1 and given by

$$N^2 = -\bar{g} \left[ \frac{1}{\bar{\rho}} \frac{\partial \bar{\rho}}{\partial r} - \frac{1}{\Gamma_1 \bar{p}} \frac{\partial \bar{p}}{\partial r} \right], \quad (2.1)$$

with  $\bar{g}$  the mean gravity,  $\Gamma_1$  the adiabatic exponent,  $\bar{\rho}$  and  $\bar{p}$  the mean density and pressure. The region where IGWs propagate is visible in the right panel of Fig. 1, where we have represented the path of propagation of two g-modes, using the linear dispersion relation (e.g. Christensen-Dalsgaard 2003) :

$$\begin{cases} k_r^2 = \frac{l(l+1)}{r^2} \left( \frac{N^2}{\omega^2} - 1 \right), \\ k_h^2 = \frac{l(l+1)}{r^2}, \end{cases} \quad (2.2)$$

where  $l$  is the spherical harmonic degree and  $k_r$  and  $k_h$  the vertical and horizontal wave numbers in the WKB approximation. Oscillations are trapped in the radiative zone, between concentric spheres of radius  $r_1$  and  $r_2$  such as  $\omega = N(r_1) = N(r_2)$ .

---

<sup>1</sup> Laboratoire AIM, CEA/DSM-CNRS-Université Paris Diderot, IRFU/SAP, F-91191 Gif-sur-Yvette Cedex, France; lucie.alvan@cea.fr, allan-sacha.brun@cea.fr, stephane.mathis@cea.fr

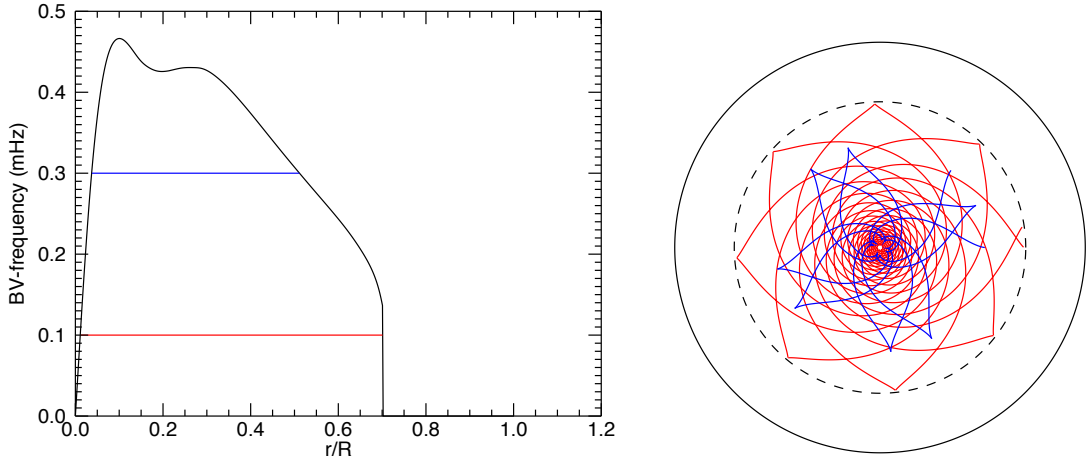


**Fig. 1. Left:** Radial profile of the Brunt-Väisälä frequency in the 1D solar model (Brun et al. 2002) taken as reference state for our 3D simulation (§3). The horizontal blue (resp. red) line indicates the trapping region for a g-mode with frequency  $\omega = 0.3$  mHz (resp.  $\omega = 0.1$  mHz). **Right:** Raypaths of gravity waves in the Sun. Waves undergo total refraction at the points where  $\omega = N$ . The dashed circle represents the base of the convective zone. The rays correspond to modes with frequency of 0.1 mHz (red) and 0.3 mHz (blue).

### 3 3D simulation

Following the work of Brun et al. (2011), we have developed a numerical 3D model of the sun coupling the convective zone with the radiative interior. As we want to focus on the propagation of IGWs, we have chosen for this new model a lower thermal diffusivity coefficient  $\kappa$ . The expected effect is to decrease the radiative damping of the waves, adapted from Zahn et al. (1997) :

$$\tau_{l,m}(r) = [l(l+1)]^{3/2} \int_r^{r_c} \kappa(1 + \text{Pr}) \frac{N^3(r')}{[\omega + m(\Omega(r') - \Omega_c)]^4} \frac{dr'}{r'^3}, \quad (3.1)$$

with  $\text{Pr} = \nu/\kappa$  the Prandtl number,  $\nu$  the viscosity coefficient and  $\Omega(r')$  and  $\Omega_c$  the mean horizontally averaged angular velocity at the point  $r'$  and at the basis of the convective zone. Figure 2 shows that the amplitude of

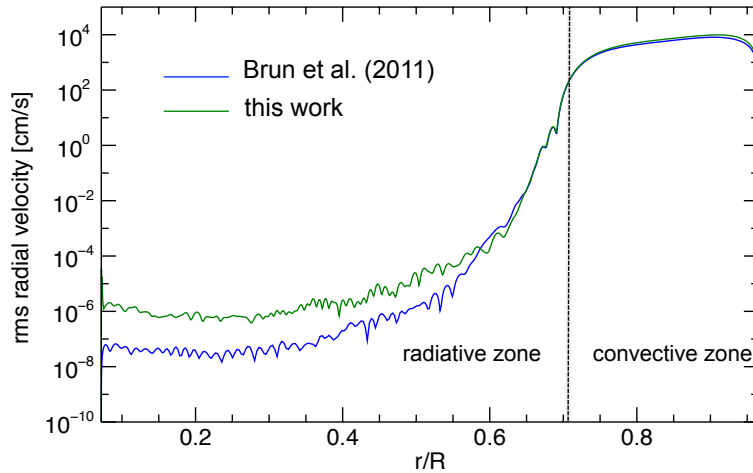


**Fig. 2.** Root mean square (rms) velocity as a function of the normalized radius for both models. The consequence of decreasing  $\kappa$  is clearly visible.

waves is indeed less attenuated in this work than in Brun et al. (2011) and hence less subject to numerical noise.

Figure 3 shows the actual displacement associated to the waves in the radiative zone. In both panels, the radial velocity  $v_r/v_{rms}$  is represented, where  $v_{rms}$  is the root mean square radial velocity at each radius. Dark blue tones (resp. red) denote downflows (resp. upflows). We clearly distinguish two regimes : a wave like pattern in the radiative zone and a large scale convection with up- and downflows in the outer convective envelope. The left panel shows phase fronts moving radially outward, which is a signature of gravity wave packets whose vertical group velocity is inward and phase velocity is outward. In the convective zone, we also note the moderate tilt of downflow lanes by the differential rotation in radius and latitude.

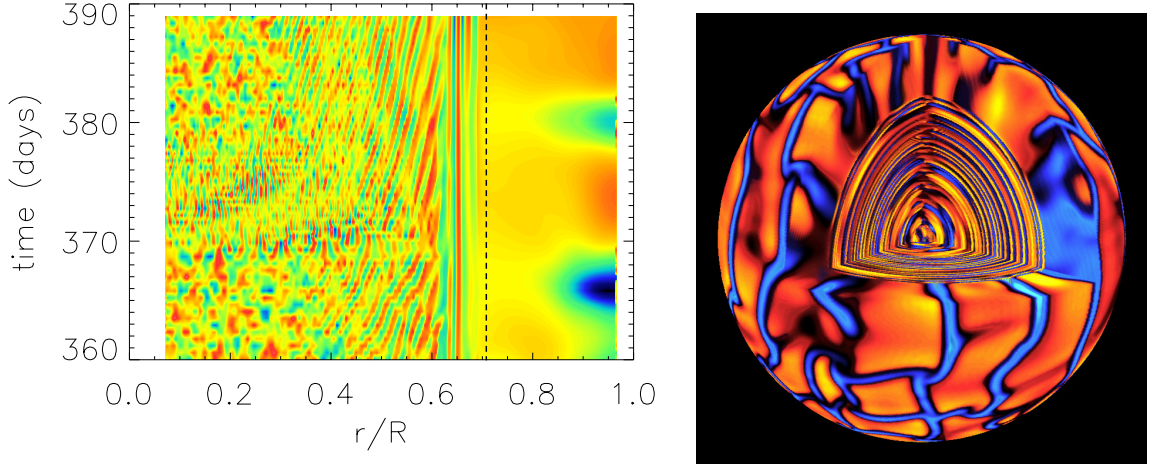


**Fig. 3. Left:** Radial velocity  $v_r/v_{rms}$  as a function of normalized radius and time. Dashed line mark the limit between radiative and convective zones according to the Schwarzschild criteria. **Right:** 3D rendering. An octant has been removed in order to visualize the structure within the meridional and the equatorial planes.

#### 4 Power spectra

To study the properties of the waves in the frequential domain, we calculate the power spectrum by computing a Spherical Harmonic transform followed by a temporal Fourier transform of the waves radial velocity. Thus, we can isolate one particular mode  $(l,m)$ . Figure 4 shows the power spectrum obtained for  $(l=1,m=0)$  and  $(l=2,m=0)$ . The normalized power is plotted as function of frequency (left) and period (right). From a theoretical point of view, the frequencies of g-modes are determined for the Bore quantization rule (e.g. Kosovichev 2011):

$$\int_{r_1}^{r_2} k_r dr = \pi(n + \alpha), \quad (4.1)$$

where  $r_1$  and  $r_2$  are the radii of the inner and outer turning points where  $k_r = 0$ ,  $n$  is the radial order (integer number) and  $\alpha$  is a phase shift which depends on the properties of the reflecting boundaries. Far from the turning points ( $N \gg \omega$ ),

$$k_r \approx \frac{\sqrt{l(l+1)} N}{r \omega}, \quad (4.2)$$

and in the asymptotic limit  $n \gg l$ , Gough (1993) shows that the spectrum of g modes is approximately equidistant with the period spacing

$$(\Delta P)_l = \frac{\pi}{\sqrt{l(l+1)} \int_{r_{bot}}^{r_{top}} \frac{N}{r} dr}, \quad (4.3)$$

$r_{bot}$  and  $r_{top}$  being the lower and upper boundaries of the radiative zone. Since we are not yet able to deal with the singularity in  $r = 0$ , the inner boundary of our computational domain is  $r_{bot} \approx 0.07R_\odot$ . The outer boundary is  $r_{top} \approx 0.71R_\odot$ . Comparing the value of  $(\Delta P)_l$  given by Eq. (4.3) with the one measured in Fig. 4, we obtain a qualitative agreement summarized in Tab. 1.

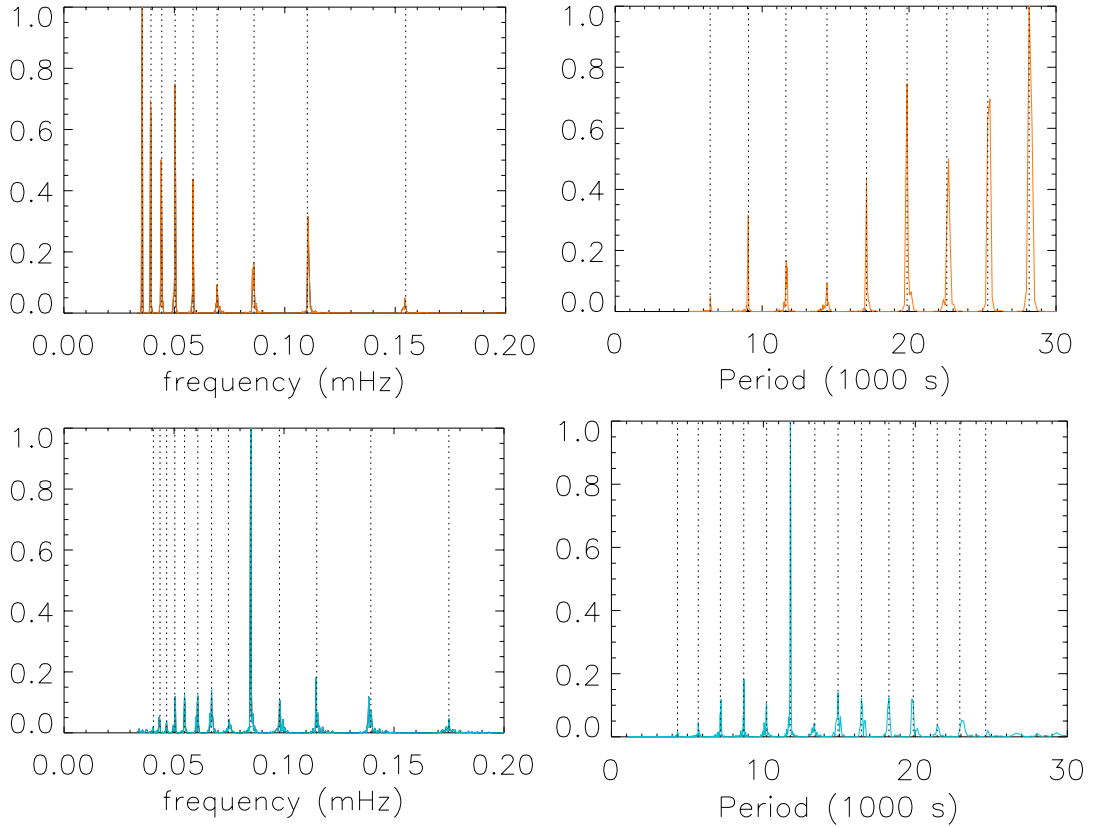


**Fig. 4.** Power spectra of the radial velocity for the modes  $(l=1, m=0)$  (orange) and  $(l=2, m=0)$  (blue). Vertical dashed lines mark the spacing between peaks.

**Table 1.** Comparison between  $(\Delta P)_l$  given by Eq. (4.3) and  $(\Delta P)_l$  from simulated data.

$(l, m)$	$(\Delta P)_l$ from Eq. (4.3)	$(\Delta P)_l$ from simulation
(1,0)	2410 s	$2713 \pm 96$ s
(2,0)	1391 s	$1560 \pm 111$ s

According to Eq. (4.1) and (4.2), we have

$$\omega \propto \int_{r_{\text{bot}}}^{r_{\text{top}}} \frac{N}{r}. \quad (4.4)$$

Since the central cut-off modifies the cavity by 10% in radius, it induces a frequency change of about 37% (due to the large area of the integral near the center). Work is in progress to model full sphere 3D solar models with our new ASH-FD code in order to improve our ability of modeling IGWs.

## 5 Conclusions

We here open a large field of investigation concerning detailed analysis of IGWs in 3D non-linear dynamical simulations. For example, we show only axisymmetric modes ( $m=0$ ) but a comparison with other values of  $m$  will highlight the existence of a rotational splitting. Moreover, it is interesting to compare our results with the theoretical solutions of the eigenvalue problem. Lastly, these simulations should help to study the angular momentum transport in radiative zones and to better understand the evolution of stellar rotation. These points will be discussed in forthcoming publications.

**References**

- Brun, A. S., Antia, H. M., Chitre, S. M., & Zahn, J.-P. 2002, *A&A*, 391, 725
- Brun, A. S., Miesch, M. S., & Toomre, J. 2004, *ApJ*, 614, 1073
- Brun, A. S., Miesch, M. S., & Toomre, J. 2011, *ApJ*, 742, 79
- Charbonnel, C. & Talon, S. 2005, *Science*, 309, 2189
- Christensen-Dalsgaard, J. 2003, *Stellar Oscillations*, <http://users-phys.au.dk/jcd/oscilnotes/>
- Garcia, R. A., Turck-Chièze, S., Jiménez-Reyes, S. J., et al. 2007, *Science*, 316, 1591
- Gough, D. O. 1993, in *Astrophysical Fluid Dynamics - Les Houches 1987*, ed. J.-P. Zahn & J. Zinn-Justin (Elsevier), 399–560
- Kosovichev, A. G. 2011, *Lecture Notes in Physics*, ed. J.-P. Rozelot & C. Neiner, Vol. 832 (Berlin, Heidelberg: Springer)
- Mathis, S. 2009, *A&A*, 506, 811
- Rogers, T. M. & Glatzmaier, G. A. 2005, *ApJ*, 620, 432
- Zahn, J.-P., Talon, S., & Matias, J. 1997, *A&A*, 322, 320